2D Hexagonal Boron Nitride (2D-hBN) Explored as a Potential Electrocatalyst for the Oxygen Reduction Reaction

Aamar F. Khan[1], Dale A. C. Brownson[1], Xiaobo Ji[2], Graham C. Smith[3] and Craig E. Banks[1*]

1. Faculty of Science and Engineering, Manchester Metropolitan University, Manchester, UK
2. College of Chemistry and Chemical Engineering, Central South University, Changsha, PR China
3. Faculty of Science and Engineering, Department of Natural Sciences, University of Chester, Chester, UK

*Author for communications:

Tel: +44 161 247 1196, e-mailc.banks@mmu.ac.uk, www.craigbanksresearch.com

Abstract

Crystalline 2D hexagonal Boron Nitride (2D-hBN) is explored as a potential electrocatalyst towards the oxygen reduction reaction (ORR) when electrically wired *via* a drop-casting approach upon a range of carbon based electrode surfaces; namely, glassy carbon (GC), boron-doped diamond (BDD), and screen-printed graphitic electrodes (SPEs). We consider the ORR in acidic conditions and critically evaluate the performance of unmodified and 2D-hBN modified electrodes, implementing coverage studies (commonly neglected in the literature) in order to ascertain the true impact of this novel nanomaterial. The behaviour of 2D-hBN towards the ORR is shown to be highly dependent upon both the underlying carbon substrate and the coverage/mass utilised. 2D-hBN modified SPEs are found to exhibit the most beneficial response towards the ORR, reducing the peak potential by *ca*. 0.28 V when compared to an unmodified/bare SPE. Such improvements at this supporting substrate are inferred due to favourable 2D-hBN interaction with ridged surfaces exposing a high proportion of edge regions/sites, where conversely, we show that relatively smooth substrate surfaces (such as GC) are less conducive towards successful 2D-hBN immobilisation. In this paper, we reveal for the first time (in the specific case of using a rough supporting substrate) that 2D-hBN gives rise to beneficial electrochemical behaviour towards the ORR. Unfortunately, this material is not considered an electrocatalyst for use within fuel cells given that the estimated number of electrons transferred during the ORR ranges between 1.90–2.45 for different coverages, indicating that the ORR at 2D-hBN predominantly produces hydrogen peroxide. 2D-hBN does however have potential and should be explored further by those designing, fabricating and consequently electrochemically testing modified electrocatalysts towards the ORR.

1 Introduction

As the availability of natural energy resources depletes, it has become increasingly important to find alternative means of energy production [1]. The most common alternatives to fossil fuels are renewable sources such as hydroelectric power and wind turbines, and for transportation purposes, electrolysers for fuel cells. The latter is an electrochemical device that relies on the oxidation of a fuel, such as methanol, at a working electrode (anode), while the protons liberated act as a reducing agent to oxygen in the cathodic part of the fuel cell. Research into proton exchange membrane (PEM) fuel cells, in which the oxygen reduction reaction (ORR) occurs, is directed towards improving power output, efficiency, and longevity, such that devices become viable for the transportation fuel cell market [2].

The ORR occurs at the cathode of PEM fuel cells and has proved to be problematic (dependent upon the catalyst utilised), primarily limiting the lifetimes of devices due to electrode fouling [3, 4]. For example, PEM fuel cell degradation [2] is synonymous with the ORR due to the formation of hydrogen peroxide (H_2O_2) when using catalysts that reduce oxygen *via* a two electron pathway [5]. Furthermore, slow electron transfer kinetics during the ORR can potentially result in a 50 % voltage loss and reduce the performance of a PEM fuel cell [2, 6]. There are also problems related to the relative costs of fuel cell catalysts, with platinum (Pt) [7] favoured due to its direct four electron pathway that does not produce harmful by-products such as H_2O_2 [8]. Consequently, research is directed towards discovering cheaper non-precious metal catalysts [9] and more pertinently, metal-free carbon materials. Of note, carbon based electrodes have been explored as potential metal-free electrocatalysts for the ORR with limited success given that processes proceed *via* the unfavourable two electron pathway (producing H_2O_2) [5].

With the above insights in mind, we consider the ORR using crystalline hexagonal 2D-hBN, a 2D nanomaterial comprising equal boron and nitrogen atoms arranged in a similar hexagonal structure in crystalline form to that of graphene (thus referred to as ‘white graphene’) [10]. 2D-hBN is found in amorphous and crystalline forms [11], with crystalline 2D-hBN containing strong σ bonds and weak van der Waals forces [12], resulting in a range of favourable thermal, mechanical, and chemical properties [13]. Resultantly, 2D-hBN has been widely researched in the field of electrochemistry for applications such as composites, dielectrics and optics [12]. However, note that the bonding of 2D-hBN is covalent [12] and the electrons in the σ bond are localised towards nitrogen [12], whereas the π bonding present involves an empty p-orbital of boron and a filled p-orbital of nitrogen, with the nitrogen π electrons delocalised [12]. Such an electronic structure allows 2D-hBN to be a good insulator in its solid form [14].

Considering PEM fuel cells, it has recently been reported that a 2D-hBN membrane permits protons through its structure whilst simultaneously reducing fuel crossover [15]. This effect is highly desirable and may help to improve fuel cell lifetime. However, the report does not consider that 2D-hBN *per se* may be useful as a catalytic material for fuel cell cathodes. In this regard, there have been limited investigations of 2D-hBN as an electrode material. Koitz et al. [16] computationally investigated the ORR with 2D-hBN supported upon Co, Ni, and Cu and found that the underlying metal support highly influenced the reaction energetics, with 2D-hBN/Cu showing a particularly low potential for the ORR to occur. Furthermore, Lyalin et al. [17] found *via* density functional theory (DFT) calculations that an inert 2D-hBN monolayer can become catalytically active upon nitrogen doping, whilst Studt et al. [18] explored the effects of nitrogen doped graphene towards the ORR with DFT calculations and

found the intermediates involved in the reaction bind to the carbon atom next to the nitrogen dopant. In other work, Uosaki et al. [4] experimentally investigated the ORR and immobilised 2D-hBN upon gold substrates/electrodes. Their work demonstrated an excellent 2D-hBN|gold interaction due to the binding of the 2D-hBN monolayer with transition metal surfaces, resulting from the interaction between the N-p_z and B-p_z orbitals of 2D-hBN and the d_z^2 orbitals [4]. Thus upon modification of a gold electrode with 2D-hBN, the potential required for the ORR was reduced by *ca*. 0.27 V compared to a bare gold electrode (although unfortunately the modified electrode followed the two electron pathway, producing H_2O_2) of the gold electrode [4]. This example shows that 2D-hBN potentially possesses an electrocatalytic behaviour towards the ORR on this substrate. However, gold is a precious metal with a high cost, making it an expensive substrate and therefore not highly desirable in the design and commercialisation of fuel cells [4].

Investigations of 2D-hBN immobilised on carbon-based substrates is perhaps a more pertinent research direction for this material, as is the theme of this paper. To the best of our knowledge, 2D-hBN has yet to be reported to exhibit an electrocatalytic behaviour (or an improved electrochemical response) when immobilised upon a carbon substrate towards the ORR [4, 19]. Previous reports have failed to identify 2D-hBN masses that give rise to beneficial voltammetric behaviours (limited to metallic surfaces) [4, 16, 20], nor have they considered several underlying/supporting carbon species in terms of their electrical anisotropy or surface roughness (and substrate effects) [4]. We note that Uosaki et al. [4] investigated 2D-hBN using a glassy carbon based substrate and observed little (*no real*) electrocatalytic effect towards the ORR [4]. This paper takes a novel approach and investigates the electrocatalytic performance of different 2D-hBN coverages immobilised upon a range of carbon-based substrates (namely; glassy carbon (GC), boron doped-diamond (BDD), and screen-printed graphitic electrodes (SPEs)) towards the ORR. We compare the results to other 2D materials and noble metal electrodes such as platinum and gold for the ORR. To our knowledge 2D-hBN has, to date, not been reported as a beneficial ORR material when supported upon carbon substrates; thus, this work provides a high level of novelty.

2 Experimental

All chemicals utilised were of analytical grade and were used as received from Sigma-Aldrich without any further purification. All solutions were prepared with deionised water of resistivity not less than 18.2 MΩ cm and (when necessary) were vigorously degassed prior to electrochemical measurements with high purity, oxygen free nitrogen.

Voltammetric measurements were performed using an ‘Autolab PGSTAT 101’ (Metrohm Autolab, The Netherlands) potentiostat. All measurements were conducted, using a conventional three electrode system. The working electrodes were a screen-printed graphite electrode (SPE), a glassy carbon (GC) electrode (3 mm diameter, BAS, USA); a boron-doped diamond (BDD) electrode (3 mm diameter, BAS, USA), a platinum (Pt) electrode (3 mm diameter, BAS, USA), a gold (Au) electrode (3 mm diameter, BAS, USA), and an edge-plane pyrolytic graphite (EPPG) electrode (4.9 mm diameter, Le Carbone, Ltd., Sussex, UK, machined from a slab of highly ordered pyrolytic graphite (HOPG)). 2D-hBN modified electrodes were prepared by drop-casting aliquots of an ethanol suspension containing pristine flakes of 2D-hBN onto the required working electrode with a micropipette. After 30 minutes the ethanol completely evaporated (at ambient temperature) and the modified electrodes were ready for use. A platinum wire and a saturated calomel electrode (SCE) were

used as counter and reference electrodes, respectively. The SPE, GC, BDD, EPPG, Au and Pt working electrodes were polished with 'Kemet diamond spray' (1.00 and 0.25 micron respectively) and were thoroughly washed with deionised water prior to commencing any experiments (and before 2D-hBN modification).

The screen-printed graphite electrodes (SPEs) utilised throughout this work consisted of a graphite working electrode, a graphite counter electrode and an Ag/AgCl reference electrode. The SPEs, which have a 3 mm diameter working electrode, were fabricated in-house with appropriate stencil designs using a microDEK 1760RS screen-printing machine (DEK, Weymouth, UK). This SPE design has been previously reported [21-23]. For experimental continuity, the SPE's on-board Ag/AgCl reference and carbon counter electrodes were removed and replaced with an external SCE reference and Pt counter electrodes respectively. The SPEs have been electrochemically characterised previously and exhibit a heterogeneous electron transfer rate constant, k^{o}_{eff}, of *ca*. 1.08×10^{-3} cm s^{-1} using 1 mM hexaammineruthenium (III) chloride/0.1 M KCl [24]. The reproducibility and repeatability of the fabricated batches of electrodes were explored through comparison of cyclic voltammetric responses using 1 mM $Ru(NH_3)_6^{2+/3+}$ in 0.1 M KCl supporting electrolyte. Analysis of the voltammetric data revealed the % relative standard deviation (% RSD) to correspond to no greater than 0.82 % (N=20) and 0.76 % (N=3) for the reproducibility and repeatability of the fabricated SPEs (for use in electroanalysis) [25].

The 2D-hBN utilised was commercially obtained from 'Graphene Supermarket' (Reading, MA, USA) and is known as 'Boron Nitride Pristine Flakes' comprised entirely of pristine 2D-hBN nanoscale crystals dispersed in ethanol (5.4 mg L^{-1}) that have not been oxidised, reduced or chemically modified in anyway and are free from surfactants [29]. These are fabricated *via* a liquid exfoliation procedure using ethanol and water in appropriate composition to produce a highly stable suspension. The 2D-hBN platelets have an average particle size (lateral) of *ca*. 50–200 nm, a thickness of between 1–5 monolayers (in solution) and a purity (in the dry phase) of >99 % [29]. Typical TEM images are presented in Figure 1.

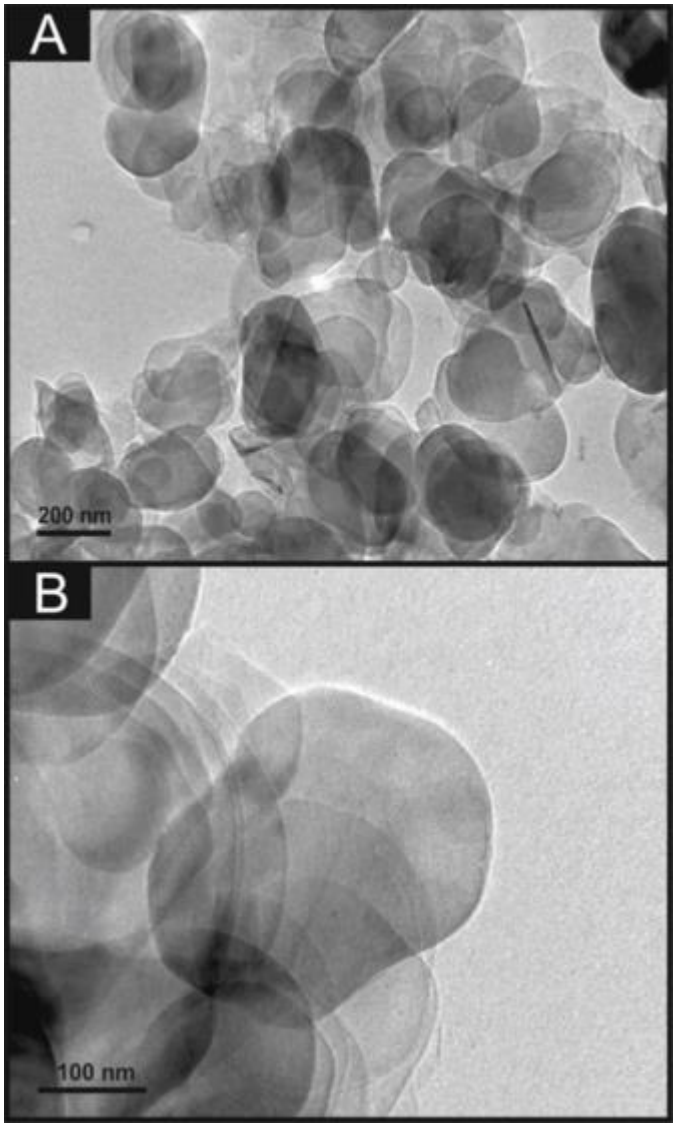

Figure 1.

Typical TEM images of commercially procured 2D-hBN deposited onto a holey carbon film supported upon a Cu TEM grid (A), and at a higher magnification (B). Scale bars are 200 nm (A) and 100 nm (B). Images obtained using a 200 kV primary beam under bright-field conditions.

For experimental procedures/tests investigating the electrochemical detection of oxygen, sulfuric acid solutions utilised were of the highest grade available from Sigma-Aldrich (99.999 %, double distilled for trace metal analysis) and was used at a concentration of 0.1 M. To oxygenate the solution, it was subject to rigorous bubbling of 100 % medicinal grade oxygen through 100 mL of the solution for 45 minutes, assuming this to be a completely saturated solution at room temperature as described by Gara [5]. The concentration of oxygen was assumed to be 0.9 mM according to previous reports using the same method [5, 8].

Where stated, the effective heterogeneous electron transfer (HET) rate constant, k^{o}_{eff} , was determined utilising a method developed by Nicholson [26], applicable for quasi-reversible systems. The following equation was used to determine the HET: $\psi=k^{o}_{eff}$ $[\pi D n \upsilon F/(RT)]^{-1/2}$,

where ψ is a kinetic parameter, D is the diffusion coefficient (D=9.1×10^{-6} cm^2 s^{-1}; for $Ru(NH_3)_6^{2+/3+}$ in 0.1 M KCl supporting electrolyte) [27], n is the number of electrons involved in the electrochemical process, F is the Faraday constant, R the universal gas constant and T the temperature. The kinetic parameter, ψ, was tabulated as a function of peak-to-peak separation (ΔE_P) at a set temperature (298 K) for a one-step, one electron process (where the transfer coefficient, α=0.5). The function of $\psi(\Delta E_P)$, which fits Nicholson′s data, for practical usage (rather than producing a working curve), is given by: $\Psi=(-0.6288+0.0021X)/(1-0.017X)$. [28] Where $X=\Delta E_p$, was used to determine ψ as a function of ΔE_P from the experimentally recorded voltammetry. From this, a plot of ψ against $[\pi D n \upsilon F/(RT)]^{-1/2}$ allowed the k^o_{eff} to be readily determined. Note that all k^o_{eff} values were deduced over the scan rate range of 15–400 mV s^{-1}.

Transmission electron microscopy (TEM) images were obtained using a 200 kV primary beam under conventional bright-field conditions. The 2D-hBN sample was dispersed onto a holey-carbon film supported on a 300 mesh Cu TEM grid. Scanning electron microscopy (SEM) images and surface element analysis were obtained using a JEOL JSM-5600LV model equipped with an energy-dispersive X-ray (EDX) for the EDX microanalysis. For Raman spectroscopy and X-ray diffraction (XRD) analysis, the 2D-hBN solution was drop-casted onto a supporting silicon wafer and dried in air. Raman spectroscopy was performed using a 'Renishaw InVia' spectrometer with a confocal microscope (×50 objective) spectrometer with an argon laser (514.3 nm excitation) at a very low laser power level (0.8 mW) to avoid any heating effects. Spectra were recorded using a 10 second exposure time for 3 accumulations. The Raman mapping was performed using a 'Thermo Scientific DXR Raman Microscope' with laser (532 nm excitation). The XRD was performed using a "X'pert powder PANalytical model" with a copper source of K_α radiation of 1.54 Å and $K_ß$ radiation of 1.39 Å, using a thin sheet of nickel with an absorption edge of 1.49 Å to absorb $K_ß$ radiation. White light profilometry was carried out using a ZeGage 3D Optical Surface Profiler, manufactured by Zygo.

X-ray photoelectron spectroscopy (XPS) was used to analyse the electrode surface and its oxygenated groups. XPS data was acquired using a bespoke ultra-high vacuum system fitted with a Specs GmbH Focus 500 monochromated Al Kα X-ray source, Specs GmbH PHOIBOS 150 mm mean radius hemispherical analyser with 9-channeltron detection, and a Specs GmbH FG20 charge neutralising electron gun. Survey spectra was acquired over the binding energy range 1100–0 eV using a pass energy of 50 eV and high resolution scans were made over the C 1s and O 1s lines using a pass energy of 20 eV. Under these conditions the full width at half maximum of the Ag $3d_{5/2}$ reference line is *ca*. 0.7 eV. In each case, the analysis was an area-average over a region approximately 1.4 mm in diameter on the sample surface, using the 7 mm diameter aperture and lens magnification of ×5. The energy scale of the instrument was calibrated according to ISO standard 15472, and the intensity scale was calibrated using an in-house method traceable to the UK National Physical Laboratory. Finally, data was quantified using Scofield photoelectric cross sections corrected for the energy dependencies of the electron attenuation lengths and the instrument transmission. Data interpretation was carried out using CasaXPS software v2.3.16.

3 Results and Discussion

3.1 Physicochemical Characterisation of 2D-hBN

The physicochemical characterisation of the 2D-hBN utilised in this work is provided through TEM, SEM, XPS, EDX, XRD and Raman spectroscopy. Typical TEM images are depicted in Figure 1 where it can be observed that 2D-hBN platelets have an average (lateral) particle size of *ca*. 200 nm, which is in agreement with the commercial manufacturer [29]. Furthermore, SEM images were obtained to assess how the 2D-hBN platelets prefer to reside upon SPE surfaces. SPEs were utilised as a model electrode surface due to the ease at which they can be adapted and placed into an SEM instrument, unlike the alternative carbon electrodes utilised in this study. Figure 2A and 2B display the surface morphology of an unpolished and polished SPE. It is clear that the polishing process reduces the number of contours and ridges of the SPE (evident in Figure 2A) to a comparatively smooth electrode surface (as observed within Figure 2B). Figure 2C–F shows how the surface morphology changes when the 2D-hBN is immobilised upon the SPE surface. In Figure 2C (unpolished SPE), the 2D-hBN platelets are visible as discs that collect preferentially around contours and ridges upon the SPE surface. Conversely, Figure 2D (polished SPE) shows the platelets collecting in similar areas, but also indicates large areas of underlying substrate where the platelets have not rested because the surface is apparently not suitable to 2D-hBN interaction, leading us to infer that 2D-hBN prefers to reside upon a rougher electrode surface. This is an interesting concept occurring following the modification of electrode surfaces with 2D-hBN and the implications of this are considered later.

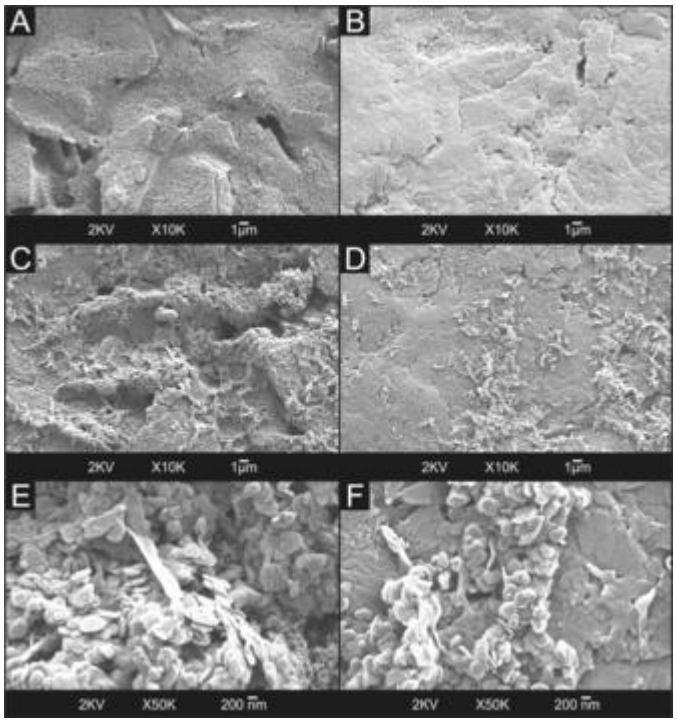

Figure 2.

Typical SEM images for: unpolished SPE (A); polished SPE (B); unpolished SPE with 324 ng 2D-hBN (C) and a further magnified version (E); polished SPE with 324 ng 2D-hBN (D) and a further magnified version (F). 2D-hBN platelets are evident in images C–F as small, disc-like shapes approximately 200 nm in size.

XPS analysis was next performed on the 2D-hBN and is depicted in ESI Figure 1. Note that the analysis was conducted on a thin layer of 2D-hBN, dried from an ethanol suspension on a Si(111) substrate and therefore the results include contributions from the underlying Si wafer,

its surface oxide and any adventitious contaminants as well as from the 2D-hBN and the ethanol residue. The XPS spectra showed the presence of a single component at 190.8 eV in the B 1s spectrum and the N 1s spectrum exhibited a main peak at 398.4 eV, with both in good agreement to previous literature [30]. A weak (minor) component in the N 1s spectrum at *ca*. 400.2 eV was evident and most likely originated from atmospheric contamination on the underlying Si(111) substrate. Thus, the results are fully consistent with 2D-hBN immobilised upon a Si(111) substrate. The stoichiometry of 1 : 1 for B : N is noted and the binding energies for the B 1s and N 1s photoelectron peaks agree well with the expected values for 2D-hBN. ESI Table 1 exhibits the full surface composition of the dried ethanol suspension of 2D-hBN on Si(111) from the XPS analysis. The C and O present are likely a result of residuals from the ethanol used to disperse the 2D-hBN. The presence of a C−O component in the C 1s spectrum (not shown) confirmed this. The Na and Ca were attributed to the concentration of Na- and Ca-containing contaminants in the ethanol. The Si and a proportion of the O originated form the Si(111) wafer substrate, which typically has thin surface oxide of approximately 1.5 nm thickness. The XPS analysis confirmed the presence of stoichiometric 2D-hBN in the commercially obtained material.

It has previously been shown that metallic impurities in carbon nanotubes can contribute to the electrocatalysis seen at some nanotube-modified electrodes [31]. Thus, it is important to consider the possible presence of metallic impurities for the case of 2D-hBN, which if present, may contribute to the response observed towards the ORR. EDX analysis was performed on a single platelet of 2D-hBN (see ESI Figure 2) to further establish its elemental composition, where it was indicated to be comprised of 11.40 % atomic boron and 9.93 % atomic nitrogen. This is in agreement with the XPS obtained that shows the stoichiometry between B : N is *ca*. 1 : 1. Further scrutiny of the EDX data reveals a 78.67 % contribution/component of atomic silicon, which as discussed above originates from the substrate upon which 2D-hBN is immobilised. This confirms that there are no impurities within our commercially obtained samples, therefore the response is not dominated by such metallic constituents, but rather is due solely to that of the 2D-hBN present.

XRD was performed on the 2D-hBN with corresponding spectra depicted in ESI Figure 3, indicating that 2D-hBN crystals are oriented in the (002) direction with a characteristic peak observed at 26.7°, in agreement with an independent literature report [32].

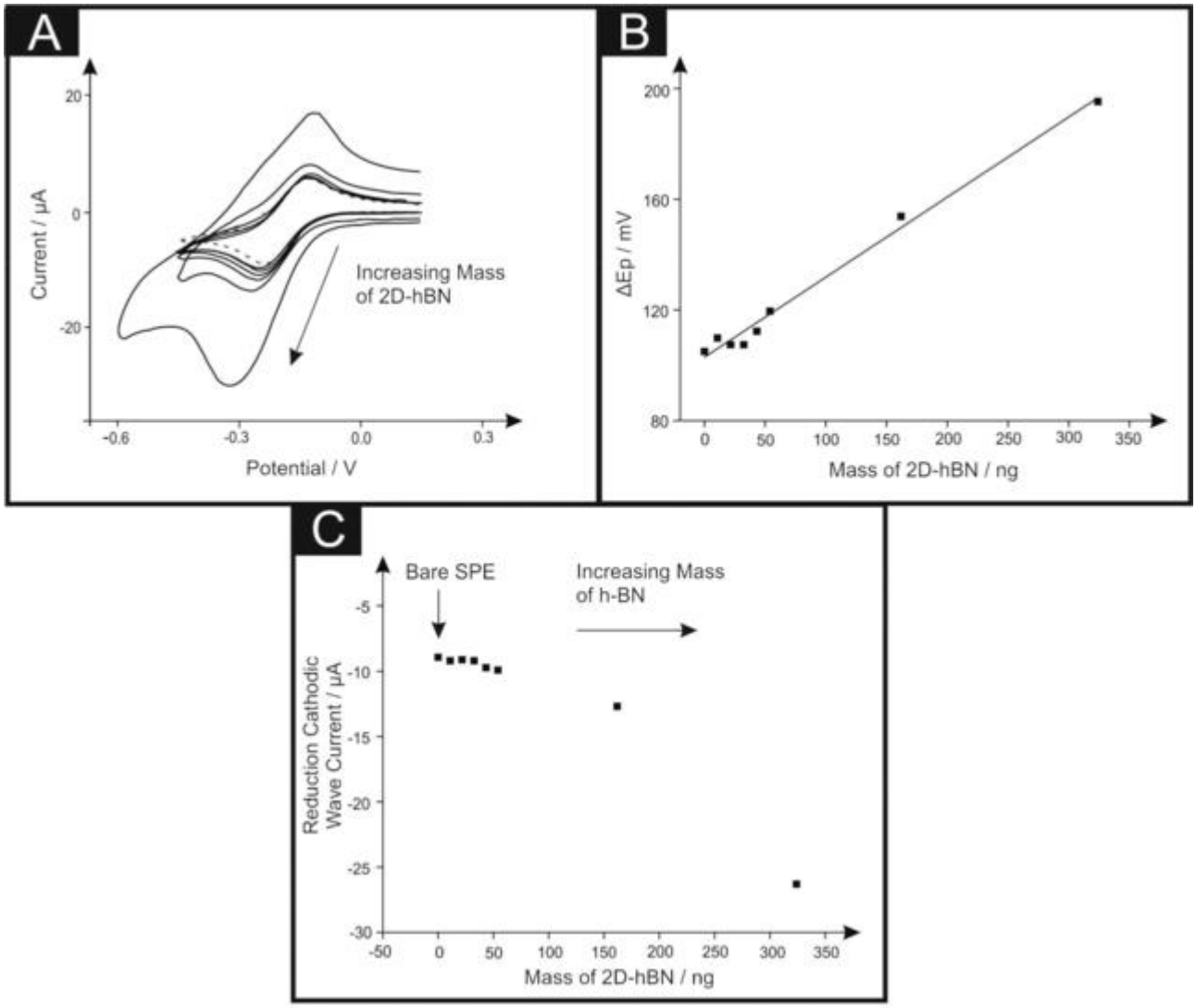

Figure 3.

Typical cyclic voltammograms (A) recorded in 1 mM $[Ru(NH_3)_6]^{2+/3+}$/0.1 M KCl with 2D-hBN masses of: 10.8, 21.6, 32.4, 43.2, 54.0, 162.0 and 324.0 ng immobilised upon SPEs. The dotted line represents an unmodified (bare) SPE. Also shown is the analysis of the voltammograms presented in Figure 3A in the form of peak-to-peak separation (ΔE_P) *vs*. mass of 2D-hBN (B) and 'reduction cathodic wave current' against mass of 2D-hBN (C). Scan rate: 100 mV s^{-1} (*vs*. SCE).

Finally, the commercially procured 2D-hBN was characterised using Raman spectroscopy. ESI Figure 4A shows Raman spectra of immobilised 2D-hBN upon a silicon wafer, which gives rise to a characteristic Raman peak at 1365 cm^{-1}, which is due to the E_{2g} phonon mode [33]. This is in good agreement to an independent literature report [33], indicating that the immobilised sample upon the silicon wafer consists of *ca*. 2–4 layers of 2D-hBN. Note however, it is not possible to observe the Raman peak of 2D-hBN upon graphitic electrodes due to overlapping signals occurring between 2D-hBN and graphite. Hence, we cannot refer to the 2D-hBN modified electrode in terms of the number layers immobilised upon it, but rather the mass of 2D-hBN that has been immobilised each time. Next, several masses of 2D-

hBN were immobilised upon SPEs. These modified SPEs were characterised using Raman spectroscopy (mapping) to ensure full electrode coverage of 2D-hBN. ESI Figures 4B and 4C show Raman map comparisons of an unmodified and a 324 ng 2D-hBN modified SPE. ESI Figure 4B shows a smooth/uniform surface, yet ESI Figure 4C shows several areas, appearing as black dots (and generally has a darker grey background intensity), that are indicative of 2D-hBN immobilisation given that the Raman intensities were recorded at the wavenumber corresponding to the peak observed in ESI Figure 4A. The Raman maps indicate a significant coverage of *ca*. 2 layer (thin layer) 2D-hBN on the electrode surface (with some areas that are darker in colour (higher Raman intensity) indicating occasional thicker regions (≥2–4 layers) [27]. It is clear that following 2D-hBN modification *via* drop casting, a complete coverage is achieved and thus the electrochemical profiles associated with 2D-hBN modified electrodes are due to the 2D-hBN and not the underlying electrode surface.

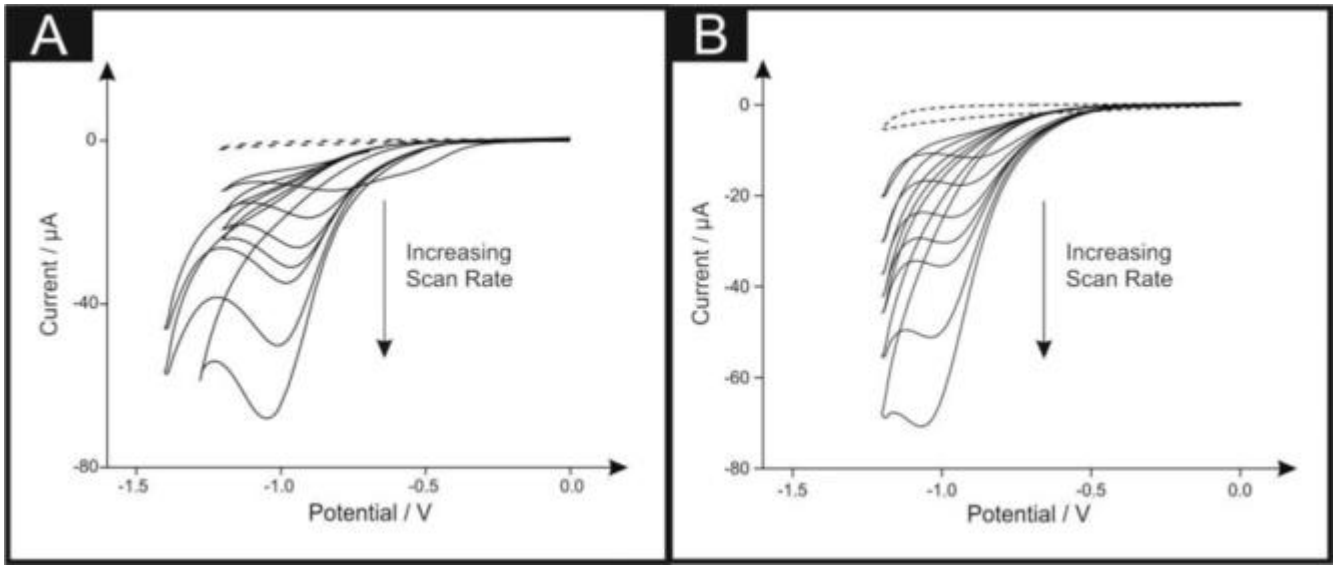

Figure 4.

Typical cyclic voltammograms recorded in oxygen saturated 0.1 M H_2SO_4 using a 108 ng 2D-hBN (A) and a 324 ng 2D-hBN (B) modified GC electrode. The dotted line depicts a deoxygenated GC electrode equivalent in each case. Scan rates: 10, 25, 50, 75, 100, 200 and 400 mV s^{-1} (*vs*. SCE).

In summary, physicochemical characterisation indicates that the material exhibits the characteristic features of highly pure 2D-hBN (no metallic impurities present), whilst comprising an average particle size (lateral) of *ca*. 200 nm and flake thickness of 2–4 layers. The drop-casting procedure appears to be an adequate method to apply/immobilise the 2D-hBN upon an electrode substrate in order to 'electrically wire to' and explore its electrochemical properties/performance, providing uniform/full coverage across the electrode surface when immobilised.

3.2 Electrochemical Characterisation of 2D-hBN

The electrochemical characterisation of 2D-hBN is considered using the outer-sphere redox probe, hexaammineruthenium (III) chloride, as a model electrochemical system. This one

electron system is used to understand its fundamental interaction with simple redox systems prior to closer examination with a more complex electrode process (ORR). Figure 3A depicts the cyclic voltammograms obtained using 2D-hBN modified SPEs, where evidently the bare electrode exhibits a peak-to-peak separation (ΔE_P) of 105 mV. It is observed that the ΔE_P incrementally shifts from *ca*. 105 to 195 mV with increasing 2D-hBN modifications from 10.8 to 324.0 ng. Using the linear gradient plotted in Figure 3B, (y=0.2892x+102.91), it is found that 50 ng of 2D-hBN increases the ΔE_P on average by 14.5 mV.

It is important to determine the effective HET rate constant, k^o_{eff}, and how modification of SPEs with different masses of 2D-hBN affects the electron transfer process occurring. The k^o_{eff} values were found to correspond to: 3.05×10^{-3} cm s^{-1} (unmodified SPE); 2.55×10^{-3} cm s^{-1} (54 ng 2D-hBN modified SPE); 1.54×10^{-3} cm s^{-1} (162 ng 2D-hBN modified SPE); and 1.09×10^{-3} cm s^{-1} (324 ng 2D-hBN modified SPE). The HET reduces as a function of 2D-hBN mass deposition, indicating that the electrochemical process is less favourable at 2D-hBN in comparison to the underlying (bare) electrode.

Despite the above observation, it is clearly visible in Figure 3A that the modification of 2D-hBN upon SPEs creates an increase in the observed peak currents. Figure 3C shows that 2D-hBN increases the cathodic (reduction) wave current by *ca*. 2.15 µA per 50 ng. The increased peak current, perhaps because of an increased surface area, is an exciting observation that may be useful for improving the current density of PEM fuel cells.

We next consider the immobilisation of high masses of 2D-hBN upon SPEs, and the effect upon the electrochemical process of hexaammineruthenium (III) chloride. ESI Figure 5A depicts typical cyclic voltammetric profiles of a 324 ng 2D-hBN modified SPE, with ESI Figure 5B depicting a plot of 'peak height' *vs*. 'square root of the voltammetric scan rate'. Analysis reveals a linear response, demonstrating a diffusional process in accordance with the Randles−Ševčík equation. Furthermore, analysis of 'log peak height' (I_p) *vs*. 'log scan rate' (v) is shown in ESI Figure 5C and reveals a gradient of 0.56 (N=3), indicating the absence of any thin layer effects and confirming that the process is predominantly diffusional controlled [34, 35].

A further consideration is the stability of the 2D-hBN modified layer(s) upon the electrode surface. We address this *via* the implementation of a stability experiment in which a 162 ng 2D-hBN modified SPE was subjected to 100 repeated cycles/scans in a hexaammineruthenium (III) chloride (0.1 M KCl) solution at 100 mV s^{-1}. This experiment simulates and recreates the appropriate timescale(s) of the voltammetric tests utilised within this work and shows that the cathodic I_p and potential remained stable, with only small (*ca*. 1.93 µA and *ca*. 0.01 V) alterations occurring in the recorded signal over 100 cycles (see ESI Figure 6 and ESI Table 2). Clearly, at this representative coverage, the 2D-hBN modified layer(s) are stable on the electrode surface and do not appear to fall off the electrode into the solution.

Next, we explore a range of carbon-based electrodes as underlying substrates for 2D-hBN immobilisation, with assessment of the resultant electrochemical performances. As presented in ESI Figure 7, the optimal 2D-hBN modified GC electrode exhibited a minimal increase in cathodic wave current, with the highest 2D-hBN modification (324 ng) resulting in a decreased cathodic wave current compared to that of previous modifications. This trend can also be observed in ESI Figure 8 for the case of a BDD electrode, as initial 2D-hBN deposition upon this electrode resulted in an increase in the cathodic wave current, from −16.1 µA (unmodified) to −20.1 µA (162 ng 2D-hBN), after which deposition of 324 ng 2D-

hBN on the BDD electrode gives rise to a decrease of 2.5 μA in the cathodic wave current. Interestingly, a different scenario was observed for an EPPG electrode (see ESI Figure 9). The two highest modifications displayed the lowest observable peak currents in this case, indicating that the electrocatalytic ability of 2D-hBN is dependent upon the underlying electrode substrate.

The data presented within this section shows that the underlying electrode substrate must be considered when utilising 2D-hBN as an electrode material and potential electrocatalyst, particularly in the case of smaller 2D-hBN modifications where the underlying substrate is likely to have a significant effect upon the observed electrochemistry [36]. Above, we have demonstrated that carbon based substrates, such as SPEs, may exhibit a synergistic effect when 2D-hBN is introduced on to their surface. It is thought that the interaction of 2D-hBN is a dominant factor in its ability to 'link' a substrate to a solution-based redox reaction, and that a ridged surface may be more favourable for this. Indeed, the evidence presented in this section shows that smooth support surfaces, such as GC electrodes, exhibit minimal increases in the cathodic wave current when 2D-hBN is introduced. Conversely, when using rougher, more ridged surfaces such as a SPE, the cathodic current increases significantly upon 2D-hBN addition. Furthermore, changes are exhibited in the electrode kinetics where differing trends are observed towards the ΔE_P upon 2D-hBN immobilisation on rough and smooth substrates. Therefore, it is important to note that one must take into account not only the quantity of 2D-hBN utilised, but also the underlying electrode substrate itself.

As previously indicated in Figure 2, we have provided SEM images that appear to support the aforementioned theory. To gain further insights however, the roughness factor (R_F) values for unmodified and 2D-hBN modified SPEs and GC electrodes were calculated using the double layer capacitance technique as described by Shin et al. [37]. First, unmodified, 108, 216 and 324 ng 2D-hBN modified SPEs were investigated in 0.1 M H_2SO_4 *via* cyclic voltammetry at various scan rates using a potential range of 0.01 to 0.11 V (due to this being the non-Faradaic potential window). The resultant voltammograms are presented in ESI Figure 10, with the corresponding analysis, as shown in ESI Figure 11, illustrating a plot of 'the difference between the anodic and cathodic current at 0.06 V' against 'the applied voltammetric scan rate'. The slope obtained is proportional to a value double that of the double layer capacitance [37], with the absolute calculated double layer capacitance values found to be 2.4, 77.2, 96.0 and 121.7 μF cm^{-2} for SPEs modified with 0, 108, 216 and 324 ng 2D-hBN. The respective R_F values are 1.0, 31.6, 39.4 and 49.9 for the 0, 108, 216 and 324 ng 2D-hBN modified SPEs. Clearly, the roughness factor significantly increases following 2D-hBN modification on SPEs. Comparatively, the R_F values obtained for unmodified and 2D-hBN modified GC electrodes significantly differ. ESI Figure 12 illustrates the double layer capacitance voltammograms obtained, with corresponding analysis in ESI Figure 13. Double layer capacitance values were found to be 12.9, 18.6, 25.7 and 14.5 μF cm^{-2} for 0, 108, 216 and 324 ng 2D-hBN modified GC electrodes, with the corresponding R_F values of 1.0, 1.4, 2.0 and 1.1.

Given the above insights concerning the electrochemical roughness of 2D-hBN modified SPEs and GC electrodes, it is noted that 2D-hBN adherence with a GC electrode is significantly lower in comparison to an SPE (in terms of alterations in the R_F values calculated following modification). This adds further evidence towards suggesting that a smooth surface, such as a GC electrode, would be less likely to form strong interactions with 2D-hBN, whereas a rougher surface, like that of the SPE, may increase the substrate interaction and in doing so can potentially create a larger (more accessible) electrode surface

area. Such an alteration upon the immobilisation of 2D-hBN may prove to be beneficial and agrees with observations reported in Figure 3 and ESI Figure 5.

Finally, white light profilometry was utilised to compare the surface topography of a range of substrates, namely GC, polished SPEs and unpolished SPEs. The surface of an unpolished SPE was observed to be significantly rougher (with a root mean squared value of the heights over the whole surface (SQ) of 1338.8 nm) than that of GC and polished SPEs, which had the SQ values of 7.6 and 806.6 nm respectively (see ESI Figure 14). Consequently, the effect of 2D-hBN modification was considered with respect to the underlying electrode's surface topography. ESI Figure 14D illustrates that immobilisation of 108 ng 2D-hBN upon a GC electrode results in the surface becoming rougher, with a new SQ value of 35.1 nm, indicating an increase of 27.5 nm. Comparatively, 108 ng 2D-hBN modification onto a polished SPE (ESI Figure 14E) increases the SQ value from 806.6 nm to 842.4 nm, an increase of 35.8 nm. Evidently, a minimal increase in surface roughness is observed when utilising smooth underlying surfaces, namely polished SPEs and GC electrodes. Conversely, immobilisation of 108 ng 2D-hBN upon an unpolished SPE (ESI Figure 14>F) resulted in the SQ value increasing from 1338.8 nm (unmodified SPE) to 1752.9 nm. This represents a significant increase of 414.1 nm at the unpolished (rough) SPE, which is distinct from that observed using smooth surfaces. This observation agrees well with the R_F values obtained earlier and suggests that 2D-hBN likely adheres more favourably to a rough surface than that of a smooth/polished surface. Whatever the cause of this observation, the phenomena is highly fascinating and will likely require further in-depth study that is outside the scope of this paper.

3.3 The Oxygen Reduction Reaction: 2D-hBN Modified Carbon Electrodes

Attention is now turned to exploring the ORR using 2D-hBN modified SPEs, GC, and BDD electrodes, where the underlying electrodes serve to electrochemically “wire” the 2D-hBN. First, unmodified SPEs, GC and BDD electrodes were explored towards the ORR within 0.1 M H_2SO_4 and scan rate studies were performed where the voltammetric peak height (I_p) was monitored as a function of scan rate (v). As depicted in ESI Figure 15, the reduction potential for the ORR using SPEs ranges from −0.82 V to −1.41 V at scan rates between 15–400 mV s^{-1}, showing an increase with scan rate that is indicative of a relatively slow electrode process. In the case of a GC electrode, the potential required for the ORR to occur ranges from −0.63 V to −0.87 V at scan rates between 15–400 mV s^{-1} (see ESI Figure 16), which is considerably less than the case of SPEs. Furthermore, ESI Figure 17 shows the use of unmodified BDD electrodes towards the ORR results in the absence of an observed oxygen peak, which is in agreement with previous literature [5]. Yano et al. [38] suggest that the ORR on BDD only begins upon pre-treatment of positive potentials greater than +1.4 V (*vs.* Ag/AgCl) given that the sp^2 hybridised carbon species become oxidised and mediate the ORR, with the most likely location for the sp^2 species being the grain boundaries of the sp^3 diamond structure [5, 38].

The effect of 2D-hBN immobilisation towards the ORR utilising the above noted electrodes is next considered. ESI Figure 18B illustrates that a 108 ng 2D-hBN modified SPE exhibits an improvement (decrease) in the potential required for the ORR to occur compared to the bare/underlying electrode (as shown in ESI Figure 18A). This is evidenced by the potential required for the ORR to occur shifting from −1.09 to −0.96 V (*vs.* SCE); hence a potential reduction of 0.13 V for the ORR to occur is observed (scan rate of 100 mV s^{-1}). Interestingly, GC electrodes display a detrimental effect upon immobilisation of 2D-hBN, with an increase

in the potential required for the ORR to occur (see Figure 4A). In this case, the potential required for the ORR to occur shifts from −0.78 V for an unmodified GC electrode to −0.99 V for an 108 ng 2D-hBN modified GC electrode (at 100 mV s^{-1} *vs.* SCE). This represents an increase of 0.19 V, inferring that 2D-hBN is not a catalytic material for the ORR when immobilised upon GC. Additionally, in the case of a 108 ng 2D-hBN modified BDD electrode, initiation of the ORR was again not observed (ESI Figure 19A). From these experiments, it is clear that there is a dependency of 2D-hBN towards the ORR upon the supporting electrode substrate – something which has been overlooked in the literature.

We next consider the diffusion occurring at a 2D-hBN modified substrate to ensure that the responses observed above (and later) are due only to changes in the electrode kinetics and that no mass transport alterations are convoluting the observed electrochemistry. Returning to the case of 2D-hBN modified SPEs as a representative example, ESI Figure 20 displays voltammetric curves for a 108 ng 2D-hBN modified SPE with peak analysis shown in ESI Figure 20B. A plot of 'peak height' *vs.* 'square-root of the scan rate' reveals a linear response, demonstrating a diffusional process. ESI Figure 20C shows analysis of 'log I_p' *vs.* 'log v', where a linear gradient of 0.534 (N=3) indicates the absence of any thin layer effects and represents a response that is purely diffusional [34].

We next explore the deposition of various masses of 2D-hBN immobilised on SPE, GC, and BDD electrodes and consider the effect of this towards the ORR. The exploration of different masses/coverages is an overlooked parameter which is not explored in the academic literature. SPEs were modified with 2D-hBN masses ranging from 54 ng to 324 ng; Figure 5 exhibits a plot of the 'oxygen reduction peak potential' *vs.* the 'mass of immobilised 2D-hBN'. It is observed that an increased mass of 2D-hBN deposited upon SPEs leads to a decrease in the potential required for the ORR to occur (a beneficial response), with a linear trend observed: E_p/V=9.0×10^{-4} mV ng^{-1} −1.072 mV; N=5; R^2=0.976. This was especially prevalent when high masses of 2D-hBN were deposited upon SPEs. The 324 ng 2D-hBN modification upon a SPE resulted in the ORR potential shifting from −1.09 V to −0.81 V (*vs.* SCE) at a scan rate of 100 mV s^{-1}, which is a potential shift of 0.28 V and indicates a significant reduction in the activation potential for the ORR. This reduction in activation potential clearly demonstrates the potential electrocatalytic behaviour of 2D-hBN when using underlying electrode substrates with rough surface morphologies (SPEs). In contrast, immobilisation of higher masses of 2D-hBN upon a GC electrode leads to a detrimental electrochemical response, with an increasing potential for the ORR evident when contrasted to the unmodified electrode. This indicates that a smoother supporting electrode surface does not exhibit a favourable interaction with 2D-hBN. For example, Figure 4B illustrates that the deposition of 324 ng 2D-hBN upon a GC electrode increases the potential required for the ORR to occur, with a shift from −0.78 V to −1.00 V (*vs.* SCE; scan rate: 100 mV s^{-1}), an overall unfavourable increase of 0.22 V. The SEM images in Figure 2 and white light profilometry (ESI Figure 14) support this inference. Of note, ESI Figure 19B illustrates the 324 ng 2D-hBN modified BDD electrode, resulting in no forthcoming oxygen peak and thus BDD is no longer considered within this work.

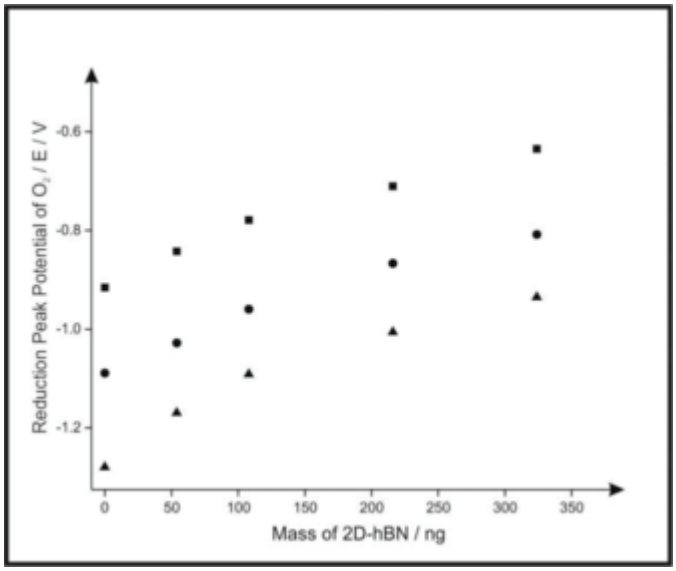

Figure 5.

Analysis of cyclic voltammograms obtained in an oxygen saturated 0.1 M H_2SO_4 solution in the form of a plot of oxygen reduction peak potential *vs*. mass of 2D-hBN deposited upon SPEs. Carried out at scan rates of 25 mV s^{-1} (square), 100 mV s^{-1} (circle) and 200 mV s^{-1} (triangle) (*vs*. SCE).

Considering the above, the voltammetric curves presented in Figure 6 demonstrate that the surface roughness has a significant bearing upon ORR performance when using 2D-hBN as a potential electrocatalyst. A smooth/polished bare SPE gives rise to a voltammetric peak at −0.77 V for the ORR, whereas a rougher, non-polished electrode exhibits a voltammetric potential of −1.16 V under identical conditions. However, in both cases the immobilisation of 324 ng 2D-hBN to the SPE surface results in a significant decrease in activation potential, and a decrease in peak current, particularly in the case of the unpolished electrode. Interestingly, in the polished (smooth) case a reduced peak potential of 0.15 V is observed, whereas the unpolished (rough) case reduces the peak potential by 0.24 V. We believe this compliments Figure 2 and ESI Figure 14, adding evidence to the argument that 2D-hBN interacts more favourably with a rougher electrode surface. This further demonstrates that 2D-hBN is not electrocatalytic for the ORR when immobilised upon a smoother substrate such as GC, which is in agreement with previous literature using gold electrodes and 2D-hBN [4].

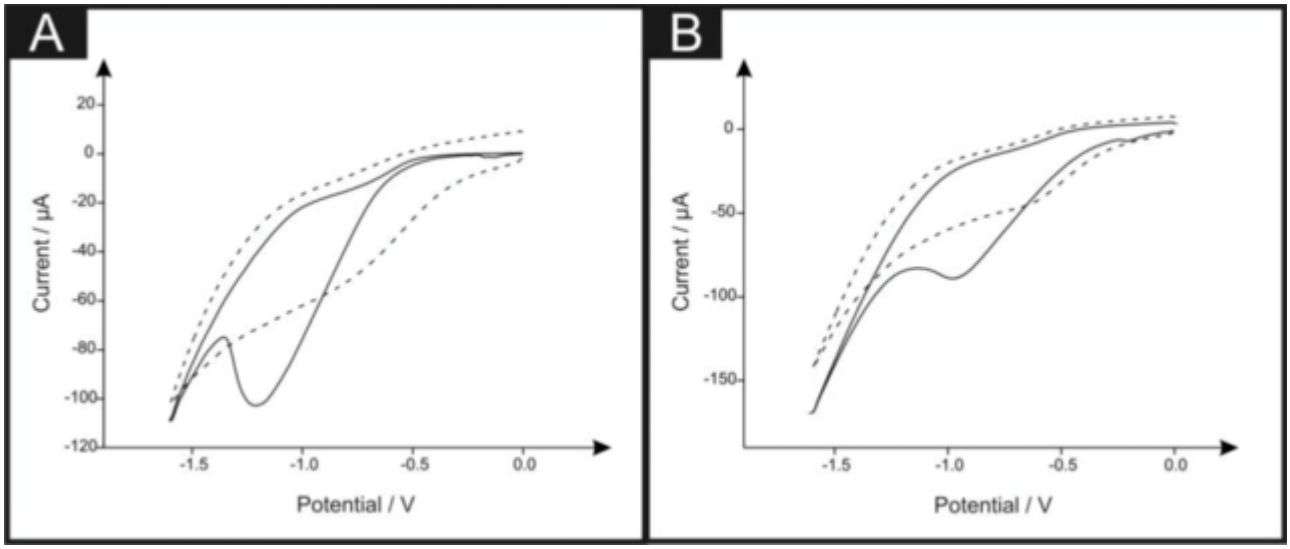

Figure 6.

Cyclic voltammograms recorded in an oxygen saturated 0.1 M H_2SO_4 solution using unmodified (A) and 324 ng 2D-hBN modified SPEs (B). The 'solid line' depicts an unpolished SPE and the 'dashed line' illustrates the response of a polished SPE. Scan rate: 100 mV s^{-1} (*vs*. SCE).

The electrocatalytic improvement of SPEs suggests 2D-hBN modified SPEs are comparable to unmodified GC electrodes for the ORR, which proceeds at *ca*. −0.78 V. This represents a valuable and important observation given that SPEs are comparatively more reproducible, cheaper to make and more readily applicable in the field than the alternative bulky GC electrode.

It is clear that the potential and performance of the ORR is dependent upon both the mass of 2D-hBN present and the roughness and electrochemical properties of the underlying electrode substrate. In prior literature where 2D-hBN was immobilised upon gold substrates, it has been demonstrated that the exposed edge regions of 2D-hBN are the active sites at which the ORR occurs [4]. In our case, rough surfaces likely expose more edge regions (and *vice versa* for the smooth surface) and are the expected origin of the apparent electrocatalytic responses observed towards the ORR. Also, note that previous reports suggest the effect of other 2D materials (namely graphene) is dependent upon the underlying electrode [39], with this clearly being the cases herein. However, this paper's purpose is to explore the potential electrocatalytic response of 2D-hBN towards the ORR and it is on this that we now focus our attention.

To gain insights into the electrochemical mechanism, Tafel analysis was performed for unmodified and 2D-hBN modified SPEs, ranging from 108–324 ng 2D-hBN. A plot of 'ln current (*I*)' *vs*. 'E_p' was constructed from analysis of the voltammograms corresponding to the electrochemical reduction of oxygen using Equation (1)

$$\frac{\delta \ln I}{\delta E} = \frac{(\alpha n')F}{RT}$$

The slope corresponds to $\delta \ln I/\delta E_p$, α is the electron transfer coefficient, F is the Faraday constant and n' is the number of electrons transferred in the rate determining step, R is the universal gas constant and T is the absolute temperature. For an unmodified SPE, the $\alpha n'$ value obtained was 0.25. Within the Tafel region, the Nernstian potential was found to increase by 165.8 mV for every order of magnitude of current. Conversely, for 108, 216 and 324 ng 2D-hBN, $\alpha n'$ values of 0.17, 0.11 and 0.11 were obtained, with a Nernstian potential increase of 113.47, 75.63 and 69.22 mV per order of magnitude of current respectively. This infers that more current flows using a 2D-hBN modified electrode than at the bare/unmodified SPE. Hence it is proposed that the transfer of the first electron is electrochemically irreversible, so n'=1 and α values of 0.25 and 0.17, 0.12 and 0.11 are obtained for the unmodified and 108, 216, 324 ng 2D-hBN modified SPEs respectively. The number of electrons transferred overall, n, was deduced using the following Randles-Ševćik equation for an irreversible electrochemical process:

$$I_p = -0.496n\,(\alpha n')^{\frac{1}{2}}\,FA[\mathrm{O_2}]\left(Fv\frac{D}{RT}\right)^{\frac{1}{2}}$$

where a literature value of 0.9 mM is anticipated for the saturated oxygen solution [8, 40], and a literature diffusion coefficient value of 2.0×10^{-5} cm^2 s^{-1} is utilised [41]. A value of n=2.73 for an unmodified SPE was obtained, whereas values of n=2.45, 2.15 and 1.90 were deduced for 108, 216 and 324 ng 2D-hBN modified SPEs respectively. Unfortunately, these values suggest that the electrochemical reduction of oxygen using unmodified and 2D-hBN modified SPEs produces hydrogen peroxide (H_2O_2) and therefore although the addition of 2D-hBN onto the SPEs improves the electrochemical response, we cannot define this material as an electrocatalyst in this case (for fuel cells). Previous studies by Uosaki et al. [4] reported that 2D-hBN followed the two electron pathway mechanism and formed H_2O_2 when immobilised upon a gold substrate for the ORR. Our work confirmed this, where the average number of electrons transferred is two, forming H_2O_2, indicating there is a similar mechanism for the ORR when utilising other 2D materials (graphene) [8].

Hydrogen peroxide (H_2O_2) yields were estimated for representative examples. First, the capacitance of an electrochemical process is estimated utilising: $C = \frac{I}{\nu}$, where C is the capacitance, I is the observed peak current at a certain potential and v is the scan rate. Next, the charge is calculated using: $Q=CV$, where Q is the charge and V is the potential. Resultantly, $Q=nFN$ enables the amount of oxygen electrolysed in the reaction to be calculated, where n is the number of electrons transferred, F is the Faraday constant and N is the number of moles of oxygen electrolysed. There is a 1 : 1 stoichiometric ratio of oxygen produced to H_2O_2, thus the concentration of oxygen electrolysed is theoretically the same as the concentration of H_2O_2 produced in the electrochemical reaction. Therefore the estimated H_2O_2 yields were calculated for an oxygenated 0.1 M H_2SO_4 solution at a fixed volume of 10 mL utilising unmodified and 2D-hBN modified SPEs of masses ranging from 108–324 ng at a scan rate of 100 mV s^{-1}. It was estimated that the concentration of H_2O_2 electrolysed when utilising unmodified SPEs was 2.51 nM, whereas 2D-hBN modified SPEs resulted in 2.78, 3.01 and 3.22 nM of H_2O_2 being produced for 108, 216 and 324 ng 2D-hBN respectively, thus an increase. This agrees with the Tafel analysis and suggests that 2D-hBN modified SPEs follow a similar mechanism to unmodified SPEs towards the ORR (given that the difference in H_2O_2 yields is minimal).

A key factor in terms of the analytical performance of sensors and energy devices is the inherent reproducibility of the response. The reproducibility of the electrode materials of

interest was thus explored in acidic conditions with different masses of 2D-hBN deposited on the SPEs. A % Relative Standard Deviation (% RSD) in the analytical signal of 9.40 % was observed for the unmodified SPE (N=3) at a scan rate of 100 mV s^{-1}. This level of reproducibility is common for printed substrates and is a drawback for SPEs as reproducibility is slightly compromised for mass production. The 54, 108, 216, and 324 ng 2D-hBN modified SPE (N=3; 100 mV s^{-1}) gave % RSD values in the analytical signal of 1.81, 8.96, 3.45, and 12.59 %, respectively. The low % RSD measurements obtained for the modified electrodes highlight the reproducibility of the drop-casting method for 2D-hBN upon SPEs.

The effect of 2D-hBN immobilised upon SPEs towards the ORR in alkali conditions has also been considered. Interested readers are referred to the ESI for further information.

3.4 Comparison to the Literature

Table 1 overviews current literature reports concerning the effect of 2D nanomaterials towards the ORR when supported upon different graphitic substrates. Randviir et al. [8] found that 20 ng modified pristine graphene immobilised upon substrates such as EPPG and the basal plane of HOPG (BPPG) resulted in an increased activation potential for the ORR under acidic conditions. In the case of the EPPG electrode, the ORR activation potential shifts from −575 mV (unmodified) to −1015 mV (20 ng pristine graphene modified), whereas the BPPG shifts from −950 mV (unmodified) to −1080 mV (20 ng pristine graphene modified). However, Qazzazie et al. [42] found nitrogen doped graphene (GN) modified GC electrodes resulted in a decrease in activation potential for the ORR in alkali conditions. The potential at which the ORR occurs shifts from −250 mV to −160 mV upon GN modification [42]. Other 2D materials such as MoS_2 have been utilised for the ORR. Zhao et al. [43] have demonstrated that MoS_2 modified GC electrodes result in the ORR occurring at −420 mV in alkaline conditions. GN modified GC electrodes resulted in the ORR occurring at −310 mV [43]. The lowest potential for the ORR to occur was observed when utilising MoS_2 and GN combined, resulting in an activation potential of −230 mV [43]. In this paper, 2D-hBN immobilised upon SPEs reduces the potential required for the ORR to occur from −1090 mV to −810 mV, thus we have a greater improvement observed in our system when contrasted/compared to those reported in the literature (that are summarised in Table 1). However, we found that 2D-hBN deposition upon GC electrodes increases the ORR activation potential from −780 mV to −1000 mV and thus it is important to consider the effect and influence of different underlying support substrates.

Table 1. Comparison of 2D nanomaterials that have been utilised for the ORR.

2D material	Underlying substrate/support material	Substrate ORR potential	2D modified substrate ORR potential	Further comments	Ref.
Pristine Graphene (monolayer platelets suspended in ethanol)	EPPG	−575 mV	−1015 mV upon 20 ng addition	Cyclic Voltammetry, scan rate 100 mV s^{-1}, O_2 saturated 0.1 M H_2SO_4	[8]

2D material	Underlying substrate/support material	Substrate ORR potential	2D modified substrate ORR potential	Further comments	Ref.
Pristine Graphene (monolayer platelets suspended in ethanol)	BPPG	−950 mV	−1080 mV upon 20 ng addition	Cyclic Voltammetry, scan rate 100 mV s^{-1}, O_2 saturated 0.1 M H_2SO_4	[8]
Quasi-Graphene	EPPG	−575 mV	−535 mV	Cyclic Voltammetry, scan rate 100 mV s^{-1}, O_2 saturated 0.1 M H_2SO_4	[8]
Quasi-Graphene	BPPG	−950 mV	−910 mV	Cyclic Voltammetry, scan rate 100 mV s^{-1}, O_2 saturated 0.1 M H_2SO_4	[8]
Thermally reduced Graphene Oxide (TRGO)	GC	−250 mV	−175 mV	Cyclic Voltammetry, O_2 saturated 0.1 M KOH rotating disc 1600 rpm	[42]
Nitrogen doped Graphene (GN)	GC	−250 mV	−160 mV	Cyclic Voltammetry, O_2 saturated 0.1 M KOH rotating disc 1600 rpm	[42]
MoS_2	GC	Not available	−420 mV	Cyclic Voltammetry, O_2 saturated 0.1 M KOH	[43]
MoS_2/Nitrogen doped Graphene (GN)	GC	Not available	−230 mV	Cyclic Voltammetry, O_2 saturated 0.1 M KOH	[43]
Nitrogen doped graphene (GN)	GC	Not available	−310 mV	Cyclic Voltammetry, O_2 saturated 0.1 M KOH	[43]
Hexagonal boron nitride (2D-hBN)	GC	−780 mV	−1000 mV upon 324 ng addition	Cyclic Voltammetry, scan rate 100	This work

2D material	Underlying substrate/support material	Substrate ORR potential	2D modified substrate ORR potential	Further comments	Ref.
Hexagonal boron nitride (2D-hBN)	SPE	−1090 mV	−810 mV upon 324 ng addition	mV s^{-1}, O_2 saturated 0.1 M H_2SO_4 Cyclic Voltammetry, scan rate 100 mV s^{-1}, O_2 saturated 0.1 M H_2SO_4	This work

3.5 The Oxygen Reduction Reaction: Metallic Electrodes (Comparison to the Literature)

It has previously been reported that 2D-hBN immobilised upon gold electrodes/substrates (electrodes prepared *via* magnetron sputtering) is beneficial towards the ORR [4]. Thus, the effect of 2D-hBN deposition towards the ORR was next considered utilising gold and Pt macroelectrodes. It was observed that immobilisation of 2D-hBN upon a gold macroelectrode resulted in the potential required for the ORR reducing by *ca*. 0.08 V in comparison to an unmodified gold electrode. However, no such effect was observed when exploring 2D-hBN modified Pt electrodes. Interested readers are referred to the ESI.

4 Conclusions

We have demonstrated, for the first time, that 2D-hBN exhibits an improved electrochemical response towards the ORR when immobilised/electrically wired upon graphitic substrates. A reduction in the ORR potential of 280 mV has been demonstrated in the best case using SPEs. 2D-hBN's beneficial electrochemistry was shown to be highly dependent upon both the underlying support substrate and the mass/coverage utilised. Given that the electrochemical response/performance of 2D-hBN is significantly influenced by the former two considerations, it is important that future research incorporating this novel nanomaterial implements control measures to ascertain 2D-hBN's dependence on mass/coverage and the underlying substrate before claiming “beneficial electrocatalysis” in other pertinent systems. For example, if a researcher has picked a smooth electrode only, such as a GC, it would appear that 2D-hBN is *NOT* beneficial – *a false result*. We have demonstrated that only rough electrode surfaces give rise to beneficial/improved ORR responses, since this likely makes the morphology of 2D-hBN upon electrode surfaces such that edge regions/sites are predominantly exposed which are the active sites [4] for the ORR.

Furthermore, we have performed Tafel analysis showing, for the first time, that when 2D-hBN is supported upon graphitic substrates it undergoes a 2-electron transfer process/pathway (range: 1.90–2.45) towards the ORR, producing predominately hydrogen peroxide. Unfortunately, due to the pathway of 2D-hBN we cannot define this material as an electrocatalyst towards the ORR for use in fuel cells. Although the 2D-hBN is not as active as

platinum towards the ORR, this work demonstrates that 2D-hBN does have potential as an electrode material, which has never before been considered as a catalyst *per se*. We note that researchers will deliberately dope carbon nanotubes with (separately) Boron and Nitrogen atoms; 2D-hBN offers a readily available "doped" material and as shown in this work, can provide electrochemically useful responses. This work indicates the potential for 2D-hBN to be utilised as a beneficial and novel electrode material towards a range of applications.

Acknowledgements

We thank the British Council for an institutional link grant (172726574) which supported this research. D. A. C. Brownson acknowledges funding from the Ramsay Memorial Fellowships Trust.

References

1 *D. A. C. Brownson, D. K. Kampouris, C. E. Banks, Journal of Power Sources 2011, 196, 4873–4885.*

2 *O. T. Holton, J. W. Stevenson, Platinum Metals Review **2013**, 57.*

3 *S. K. Bikkarolla, P. Cumpson, P. Joseph, P. Papakonstantinou, Faraday Discuss. 2014,*

4 *K. Uosaki, G. Elumalai, H. Noguchi, T. Masuda, A. Lyalin, A. Nakayama, T. Taketsugu, Journal of the American Chemical Society 2014, 136, 6542–6545.*

5 *M. Gara, R. G. Compton, New Journal of Chemistry 2011, 35, 2647–2652.*

6 *W. Sheng, H. A. Gasteiger, Y. Shao-Horn, Journal of The Electrochemical Society 2010, 157, B1529–B1536.*

7 *C. Song and J. Zhang, in PEM Fuel Cell Electrocatalysts and Catalyst Layers, ed. J. Zhang, Springer London, **2008**, DOI: 10.1007/978-1-84800-936-3_2, ch. 2, pp. 89–134.*

8 *E. P. Randviir, C. E. Banks, Electroanalysis 2014, 26, 76–83.*

9 *U. Kramm, in Encyclopedia of Applied Electrochemistry, eds. G. Kreysa, K.-i. Ota and R. Savinell, Springer New York, **2014**, DOI: 10.1007/978-1-4419-6996-5_204, ch. 204, pp. 909–918.*

10 *H. Zeng, C. Zhi, Z. Zhang, X. Wei, X. Wang, W. Guo, Y. Bando, D. Golberg, Nano Letters 2010, 10, 5049–5055.*

11 *M. Kawaguchi, S. Kuroda, Y. Muramatsu, Journal of Physics and Chemistry of Solids 2008, 69, 1171–1178.*

12 *T. Gao, L.-j. Gong, Z. Wang, Z.-k. Yang, W. Pan, L. He, J. Zhang, E.-c. Ou, Y. Xiong, W. Xu, Materials Letters 2015, 159, 54–57.*

13 *Q. Xu, L. Cai, H. Zhao, J. Tang, Y. Shen, X. Hu, H. Zeng, Biosensors and Bioelectronics 2015, 63, 294–300.*

14 *L. Britnell, R. V. Gorbachev, R. Jalil, B. D. Belle, F. Schedin, M. I. Katsnelson, L. Eaves, S. V. Morozov, A. S. Mayorov, N. M. R. Peres, A. H. Castro Neto, J. Leist, A. K. Geim, L. A. Ponomarenko, K. S. Novoselov, Nano Letters 2012, 12, 1707–1710.*

15 *S. Hu, M. Lozada-Hidalgo, F. C. Wang, A. Mishchenko, F. Schedin, R. R. Nair, E. W. Hill, D. W. Boukhvalov, M. I. Katsnelson, R. A. W. Dryfe, I. V. Grigorieva, H. A. Wu, A. K. Geim, Nature 2014, 516, 227–230.*

16 *R. Koitz, J. K. Norskov, F. Studt, Physical Chemistry Chemical Physics 2015, 17, 12722–12727.*

17 *A. Lyalin, A. Nakayama, K. Uosaki, T. Taketsugu, Physical Chemistry Chemical Physics 2013, 15, 2809–2820.*

18 *F. Studt, Catalysis Letters 2013, 143, 58–60.*

19 *G. Elumalai, H. Noguchi, K. Uosaki, Physical Chemistry Chemical Physics 2014, 16, 13755–13761.*

20 *A. Lyalin, A. Nakayama, K. Uosaki, T. Taketsugu, The Journal of Physical Chemistry C, 2013, 117, 21359–21370.*

21 *N. A. Choudry, D. K. Kampouris, R. O. Kadara, C. E. Banks, Electrochemistry Communications 2010, 12, 6–9.*

22 *M. Khairy, D. K. Kampouris, R. O. Kadara, C. E. Banks, Electroanalysis 2010, 22, 2496–2501.*

23 *E. P. Randviir, D. A. C. Brownson, J. P. Metters, R. O. Kadara, C. E. Banks, Physical Chemistry Chemical Physics 2014, 16, 4598–4611.*

24 *J. P. Metters, R. O. Kadara, C. E. Banks, Sensors and Actuators B: Chemical 2012, 169, 136–143.*

25 *F. E. Galdino, C. W. Foster, J. A. Bonacin, C. E. Banks, Analytical Methods 2015, 7, 1208–1214.*

26 *R. S. Nicholson, Analytical Chemistry 1965, 37, 1351–1355.*

27 *D. A. C. Brownson, S. A. Varey, F. Hussain, S. J. Haigh, C. E. Banks, Nanoscale 2014, 6, 1607–1621.*

28 *D. A. C. Brownson, D. K. Kampouris, C. E. Banks, Chemical Society Reviews 2012, 41, 6944–6976.*

29 *Graphene Supermarket, https://graphene-supermarket.com, accessed; 04/01/2015.*

30 *L. Song, L. Ci, H. Lu, P. B. Sorokin, C. Jin, J. Ni, A. G. Kvashnin, D. G. Kvashnin, J. Lou, B. I. Yakobson, P. M. Ajayan, Nano Letters 2010, 10, 3209–3215.*

31 *C. E. Banks, A. Crossley, C. Salter, S. J. Wilkins, R. G. Compton, Angewandte Chemie International Edition 2006, 45, 2533–2537.*

32 *G. R. Bhimanapati, D. Kozuch, J. A. Robinson, Nanoscale 2014, 6, 11671–11675.*

33 *R. V. Gorbachev, I. Riaz, R. R. Nair, R. Jalil, L. Britnell, B. D. Belle, E. W. Hill, K. S. Novoselov, K. Watanabe, T. Taniguchi, A. K. Geim, P. Blake, Small 2011, 7, 465–468.*

34 *I. Streeter, G. G. Wildgoose, L. Shao, R. G. Compton, Sensors and Actuators B: Chemical 2008, 133, 462–466.*

35 *D. A. C. Brownson, A. C. Lacombe, M. Gomez-Mingot, C. E. Banks, RSC Advances 2012, 2, 665–668.*

36 *D. A. C. Brownson, C. E. Banks, The Handbook of Graphene Electrochemistry, Springer, London, 2014.*

37 *S. Shin, Z. Jin, D. H. Kwon, R. Bose, Y.-S. Min, Langmuir 2015, 31, 1196–1202.*

38 *T. Yano, E. Popa, D. A. Tryk, K. Hashimoto, A. Fujishima, Journal of The Electrochemical Society, 1999, 146, 1081–1087.*

39 *D. A. C. Brownson, L. J. Munro, D. K. Kampouris, C. E. Banks, RSC Advances 2011, 1, 978–988.*

40 *T. Kaskiala, Minerals Engineering 2002, 15, 853–857.*

41 *P. Han, D. M. Bartels, The Journal of Physical Chemistry 1996, 100, 5597–5602.*

42 *D. Qazzazie, M. Beckert, R. Mülhaupt, O. Yurchenko, G. Urban, Journal of Physics: Conference Series 2014, 557, 012009.*

43 *T. Gao, L.-j. Gong, Z. Wang, Z.-k. Yang, W. Pan, L. He, J. Zhang, E.-c. Ou, Y. Xiong, W. Xu, Material Letters 2015, 159, 54–57.*